Rapid cooling of the in-plane motion of two-dimensional ion crystals in a Penning trap to millikelvin temperatures

Wes Johnson [1,*] Athreya Shankar [2] John Zaris [1] John J. Bollinger [3] and Scott E. Parker[1,†]

[1]*Department of Physics, University of Colorado, Boulder, Colorado 80309, USA*
[2]*Department of Instrumentation and Applied Physics, Indian Institute of Science, Bangalore 560012, India*
[3]*National Institute of Standards and Technology Boulder, Boulder, Colorado 80305, USA*

We propose a highly feasible technique with no experimental overhead to rapidly cool the in-plane degrees of freedom of large two-dimensional ion crystals in Penning traps. Through simulations, we demonstrate that our approach enables the in-plane modes to cool down to a temperature of around 1 mK in less than 10 ms. Our technique relies on near-resonant coupling of the poorly cooled in-plane motions and the efficiently cooled out-of-plane motions, and is achieved without introducing additional potentials. The rapid cooling enabled by our approach is in contrast to typical operating conditions, where our simulations of the laser cooling dynamics suggest that the ion crystal's in-plane motion cools very slowly on a timescale of several hundreds of milliseconds, a rate likely slower than experimental heating rates. Our work sets the stage for sub-Doppler laser cooling of the planar motion, and more robust and versatile quantum simulation and quantum sensing experiments with two-dimensional crystals in Penning traps.

Introduction. Identifying routes to control systems with a large number of degrees of freedom is a crucial step in scaling up quantum technologies. Penning traps offer the ability to store and manipulate the electronic and motional states of a large number of ions at the quantum level [1]. Several efforts are underway to utilize two-dimensional crystals of tens to several hundreds of ions stored in Penning traps for quantum sensing and quantum information processing [2–9]. Researchers have designed protocols to simulate many-body quantum systems [10–14], studied the spread of entanglement in interacting systems [15,16], and demonstrated spin squeezing and quantum-enhanced motion sensing protocols [6,17–21]. These protocols are enabled by coupling the electronic states of the ions to their out-of-plane normal modes of vibration—called the drumhead modes—using lasers. Although the in-plane normal modes of the ions are typically not utilized in these protocols, it was shown recently that low-frequency planar modes can significantly broaden the drumhead mode spectrum if they are not cooled well [22], limiting the utility of the drumhead modes as a quantum channel for mediating ion-ion interactions.

In this Letter, we numerically demonstrate that the Doppler laser cooling of the low-frequency planar modes can be greatly improved by resonantly enhancing their coupling to the drumhead mode branch, which itself is already efficiently laser cooled [23]. Through simulations, we show that this technique can cool the low-frequency planar modes to around 1 mK in less than 10 ms. In contrast, under typical experimental conditions [6,20], our simulations reveal that these modes are cooled very slowly on a timescale of hundreds of milliseconds, which is impractical in an actual experiment where extraneous heating effects will dominate. Furthermore, we demonstrate how the efficient cooling leads to significant improvement in the resolution of the drumhead mode spectrum. By comparing our results with a simulation that removes the coupling between modes, we elucidate the role played by the resonantly enhanced coupling between the planar and drumhead modes in improving the cooling.

Setup and background. The setup we consider is shown in Fig. 1. Ions are confined in a Penning trap using a strong magnetic field $\mathbf{B} = B_0\hat{\mathbf{z}}$, and an electric quadrupole field generated by trap electrodes (not shown). Cooling lasers are applied along the x direction and the z direction to cool the planar ($\perp \mathbf{B}$) and axial ($\parallel \mathbf{B}$) motions, respectively. The planar cooling laser is offset from the trap center. Furthermore, the crystal is rotating when viewed in the laboratory frame; the role of this rotation in the laser cooling will be discussed in more detail below. To make our work concrete, we choose trap and laser cooling parameters relevant to the NIST Penning trap [6]. Details of the simulation procedure are reported in the Supplemental Material (SM) [24].

The nontrivial nature of the Doppler laser cooling in a Penning trap can be illustrated with a single trapped ion. The planar motion of a single ion is a superposition of cyclotron and magnetron modes [25,26]. Since the total energy of the magnetron mode is negative in the laboratory frame, reducing the amplitude of these motions requires that the laser must simultaneously add energy to the magnetron mode while removing energy from the cyclotron mode. This results in a fundamental cooling trade-off. The amplitude of both motions

*wes.johnson@colorado.edu
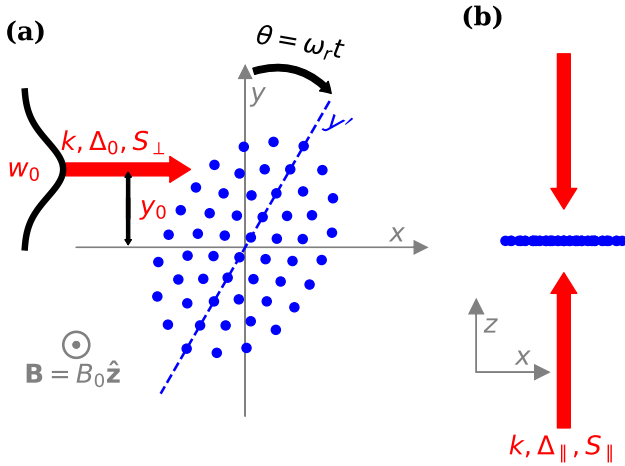†Also at Renewable and Sustainable Energy Institute, University of Colorado, Boulder.

FIG. 1. Laser cooling setup. (a) The planar laser beam. The laboratory frame coordinates are shown in gray, with the z axis chosen along the magnetic field, $B_0 = 4.458$ T, and the x axis chosen parallel to the planar laser beam, depicted in red. The ion crystal is shown in blue. A "rotating wall" potential precisely controls the rotation frequency ω_r of the ion crystal. The simulation assumes $^9\mathrm{Be}^+$ with a cooling transition wavelength $\lambda = 313$ nm. The planar beam is offset by $y_0 = 20$ μm from the center of the trap so that the laser's peak intensity occurs where the ions are receding from the laser source. The beam is assumed to have a Gaussian profile with a waist of $W_0 = 30$ μm and a saturation parameter $S_\perp = 1$. The saturation is given as a function of position, $S(y) = S_\perp \exp[-2(y - y_0)^2/W_0^2]$. The laser is red-detuned from resonance with the $^9\mathrm{Be}^+$ laser cooling transition by $\Delta_0 = -40$ MHz. (b) The axial laser beam. Two counterpropagating beams are applied along the z axis to cool the drumhead modes. Unlike in experiment, where only one beam is applied, two beams are used in simulation to cancel each other's displacement of the ion crystal's equilibrium, simplifying analysis. See the SM for details. For these beams $S_\parallel = 5 \times 10^{-3}$ to achieve axial cooling with minimal recoil heating in the planar direction. The detuning is $\Delta_\parallel = -\gamma_0/2$, where $\gamma_0 = 2\pi \times 18$ MHz is the natural linewidth of the $^9\mathrm{Be}^+$ laser cooling transition—this yields optimal cooling.

can be reduced simultaneously with a laser beam tuned to the red of the atomic ion cooling transition and an intensity gradient applied across the center of the trap [27–29]. The typical experimental method is to apply a focused planar ($\perp \mathbf{B}$) laser beam that is offset from the trap center, as is shown in Fig. 1, such that its peak intensity occurs where the magnetron motion is receding from the laser source. Measured cooling times depend on the ion species and details of the cooling laser configuration, but in Refs. [30,31], ranged from 10 to 200 ms for the magnetron motion. The measured cyclotron cooling was two to three orders of magnitude faster.

In the case of large multi-ion crystals with tens to hundreds of ions, a complete theoretical treatment of the planar laser cooling of the ion crystal is challenging. To investigate this system, we therefore perform numerical simulations using a full-dynamics integrator that includes a realistic laser cooling model [23].

In contrast to a single ion, Doppler laser cooling of multi-ion crystals in a Penning trap is complicated by the collective rotation of the crystal as viewed in the laboratory frame (see

Fig. 1). This leads to coherent Doppler shifts across the ion crystal and further limits the lowest attainable perpendicular kinetic energy ($\mathrm{KE}_\perp$) [32]. Additionally, the focused laser beam generates a torque on the ion crystal, and can change the collective rotation frequency ω_r of the ion crystal [29,33,34]. A rotating quadrupolar potential, called a "rotating wall," is applied to precisely control ω_r in experiments [35]. Energy exchange with the rotating wall potential allows for cooling of $\mathrm{KE}_\perp$ to millikelvin temperatures [34]. We chose the offset y_0 and the laser detuning Δ_0, shown in Fig. 1, to roughly minimize the laser torque for the beam width of $W_0 = 30$ μm, and to maximize the cooling of $\mathrm{KE}_\perp$ as calculated by a simple model presented in Ref. [34].

However, efficient cooling of $\mathrm{KE}_\perp$ does not necessarily imply effective cooling of the potential energy fluctuations (PE) that are associated with planar motions. The presence of a strong trapping magnetic field $\mathbf{B}$ leads to unconventional normal modes in the planar direction, which can be classified into a low-frequency $\mathbf{E} \times \mathbf{B}$ branch dominated by PE and a high-frequency cyclotron branch dominated by $\mathrm{KE}_\perp$ [22,36]. Simulations suggest that the $\mathbf{E} \times \mathbf{B}$ and cyclotron modes do not equilibrate [37], allowing the possibility for large PE to persist despite efficient cooling of $\mathrm{KE}_\perp$. This is in contrast to the drumhead modes, whose total energy is, on average, equally shared between axial kinetic energy ($\mathrm{KE}_\parallel$) and PE, and hence cooling $\mathrm{KE}_\parallel$ leads to an equal reduction of the PE. From our simulations, we find that the PE associated with planar motion is not efficiently cooled under current experimental conditions. Interestingly, as shown in Fig. 2(c), our simulations suggest the potential and kinetic energies have vastly different cooling rates. $\mathrm{KE}_\perp$ and $\mathrm{KE}_\parallel$ are cooled to millikelvin temperatures in roughly 1 ms, whereas after a brief cooling related to the reduction in $\mathrm{KE}_\parallel$, PE is not significantly cooled.

Resonant mode coupling. In order to efficiently cool the $\mathbf{E} \times \mathbf{B}$ modes, we investigate a method for sympathetically cooling these modes by resonantly coupling them to the drumhead mode branch, which itself is well cooled. For experiments utilizing a rotating wall potential, our technique is significant in that it requires no additional time-dependent potentials to engineer couplings [25,38,39], nor a change to current laser cooling setups. Instead, it relies on the observation that the frequency gap between the drumhead and $\mathbf{E} \times \mathbf{B}$ mode branches can be tuned by changing the ion crystal rotation frequency ω_r, which is a precisely controlled experimental parameter. In particular, this gap can be closed through an appropriate choice of ω_r, which leads to a resonant enhancement of the interbranch coupling.

To understand this, we consider the potential energy of the ions in a noninertial reference frame rotating with the crystal, where the total Lagrangian is time independent. This potential energy can be written as

$$U_r = \sum_{i=1}^{N} \frac{1}{2} m \omega_z^2 \left[z_i^2 + (\beta + \delta)x_i^2 + (\beta - \delta)y_i^2 \right]$$
$$+ \sum_{i=1}^{N} \sum_{j \neq i} \frac{q^2}{8\pi\varepsilon_0} \frac{1}{|\mathbf{x}_i - \mathbf{x}_j|}. \quad (1)$$
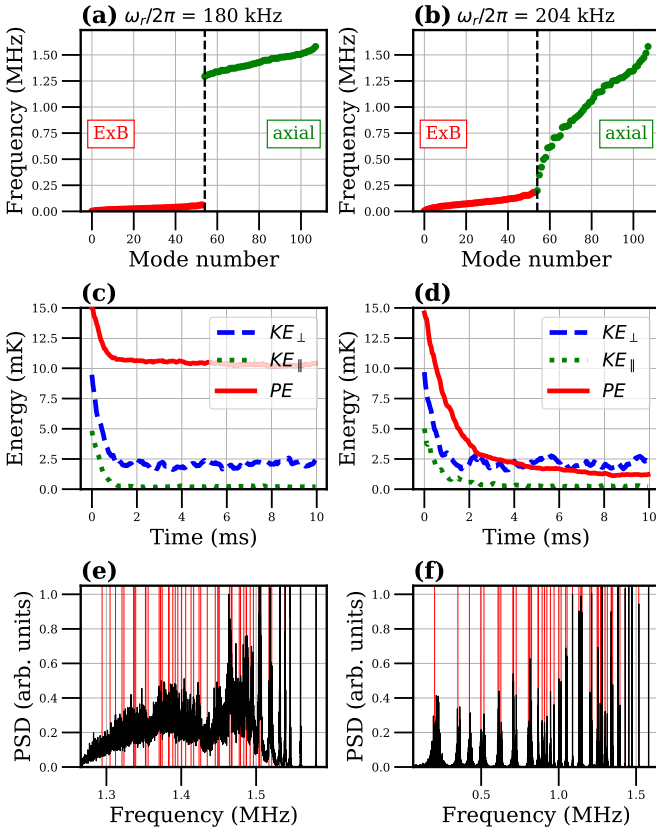
FIG. 2. Coupling of planar and drumhead modes via full simulation. A $N = 54$ ion crystal is initialized with all modes at an amplitude corresponding to a temperature of 10 mK. These simulations are evolved with the full nonlinear Coulomb interaction and laser cooling for different values of the rotating wall frequency ω_r. (a) At $\omega_r/2\pi = 180$ kHz, the $\mathbf{E} \times \mathbf{B}$ modes (left) are not resonant with the drumhead modes (right). (b) Increasing $\omega_r/2\pi$ to 204 kHz brings the $\mathbf{E} \times \mathbf{B}$ modes into resonance with the drumhead modes. (c) At $\omega_r/2\pi = 180$ kHz, the $\mathbf{E} \times \mathbf{B}$ modes are not cooled substantially in 10 ms. (d) At $\omega_r/2\pi = 204$ kHz, the $\mathbf{E} \times \mathbf{B}$ modes couple with the drumhead modes and are cooled to roughly 1 mK in 10 ms. (e) Drumhead mode spectra show broadening due to uncooled $\mathbf{E} \times \mathbf{B}$ modes. (f) Drumhead mode spectra show reduced broadening due to improved cooling of $\mathbf{E} \times \mathbf{B}$ modes.

Here, β characterizes the relative strength of planar and axial confinement and is given by

$$\beta = \frac{\omega_r(\omega_c - \omega_r)}{\omega_z^2} - \frac{1}{2}, \qquad (2)$$

where ω_c is the cyclotron frequency and ω_z is the axial trap frequency. The azimuthal asymmetry due to the rotating wall potential, which is static in this corotating frame, is parametrized by δ. In the rotating frame, the potential energy of the ions is always positive. Potential energy fluctuations are calculated as PE $= \Delta U_r$, the increase in potential energy from the crystal's equilibrium configuration. The value of β can be increased by increasing the rotating wall frequency. At a critical value $\omega_{r,\mathrm{crit}}$, where $\beta = \beta_{\mathrm{crit}}$, the planar configuration becomes unstable, and the ion crystal transitions to a three-dimensional configuration [40]. Near β_{crit} the lowest-frequency drumhead mode approaches zero, which represents

an instability of the planar ion crystal to axial displacements. In our simulations, we increase ω_r to near, but less than, ω_{crit}, such that the lowest-frequency drumhead modes are nearly resonant with the highest-frequency $\mathbf{E} \times \mathbf{B}$ modes.

Results. In Fig. 2, we show the results of simulations for an $N = 54$ ion crystal at a rotating wall frequency of $\omega_r/(2\pi) = 180$ kHz, typical of NIST work [6,20], and an increased rotating wall frequency of $\omega_r/(2\pi) = 204$ kHz. In Figs. 2(a) and 2(b), the $\mathbf{E} \times \mathbf{B}$ and drumhead mode frequencies are plotted as a function of mode number for the ion crystal simulated at these two values of ω_r. By increasing ω_r, the lowest-frequency drumhead modes are brought into resonance with the $\mathbf{E} \times \mathbf{B}$ modes. Previous numerical studies have shown that mode coupling between $\mathbf{E} \times \mathbf{B}$ modes leads to rapid equilibration of these modes [37], thus suggesting that coupling only a few $\mathbf{E} \times \mathbf{B}$ modes to drumhead modes may be sufficient to sympathetically cool the entire $\mathbf{E} \times \mathbf{B}$ mode branch. In Figs. 2(c) and 2(d), $\mathrm{KE}_\parallel$, $\mathrm{KE}_\perp$, and PE are plotted as a function of time for the two cases. These energies are calculated directly from the ion positions and velocities during the evolution of the simulations. The energies are normalized to the ion number and then converted to temperature units via $T = E/(Nk_B)$, where $E \in \{\mathrm{KE}_\parallel, \mathrm{KE}_\perp, \mathrm{PE}\}$, and k_B is the Boltzmann constant. In these simulations, we initialize the ion crystal with all mode amplitudes corresponding to 10 mK, then a random phase is chosen for each mode. Details are given in the SM. Cooling of the kinetic energies is similar in both simulations; however, the cooling of the potential energy is much faster when $\omega_r/(2\pi) = 204$ kHz. From longer simulations at $\omega_r/(2\pi) = 180$ kHz, we found that PE does cool, however, this cooling process takes hundreds of milliseconds (see SM). In contrast, Fig. 2(d) shows that PE is cooled to roughly 1 mK after 10 ms of laser cooling when $\omega_r/(2\pi) = 204$ kHz.

The improved cooling of the $\mathbf{E} \times \mathbf{B}$ modes, i.e., the PE associated with planar motion, leads to reduced fluctuations in ion positions. Consequently, the adverse impact of planar position fluctuations on the drumhead mode spectrum is greatly reduced. In Figs. 2(e) and 2(f), we plot the power spectrum of the drumhead motion for the two cases considered here, after the crystals have been laser cooled for 10 ms. For $\omega_r/(2\pi) = 180$ kHz [Fig. 2(e)], the drumhead modes are so strongly broadened that the spectrum appears as a smooth continuum beyond the first few well-resolved highest-frequency modes. In general, the sensitivity of the drumhead modes to planar position fluctuations is stronger for the lower-frequency modes. The spectrum shown in Fig. 2(e) is consistent with Fig. 7(c) of Ref. [22], which shows the broadening of the drumhead spectrum due to an in-plane temperature of 10 mK. In contrast, when $\omega_r/(2\pi) = 204$ kHz [Fig. 2(f)], the drumhead spectrum shows resolved peaks near the predicted drumhead mode frequencies over a much larger range of mode frequencies. Improving the drumhead spectral resolution could enable the use of more of these modes for high-fidelity quantum information processing protocols. So far, protocols have primarily utilized only the center-of-mass mode, which is the highest-frequency drumhead mode and is insensitive to planar position fluctuations.

To understand the role played by the mode coupling in the improved cooling, we compared our results against a
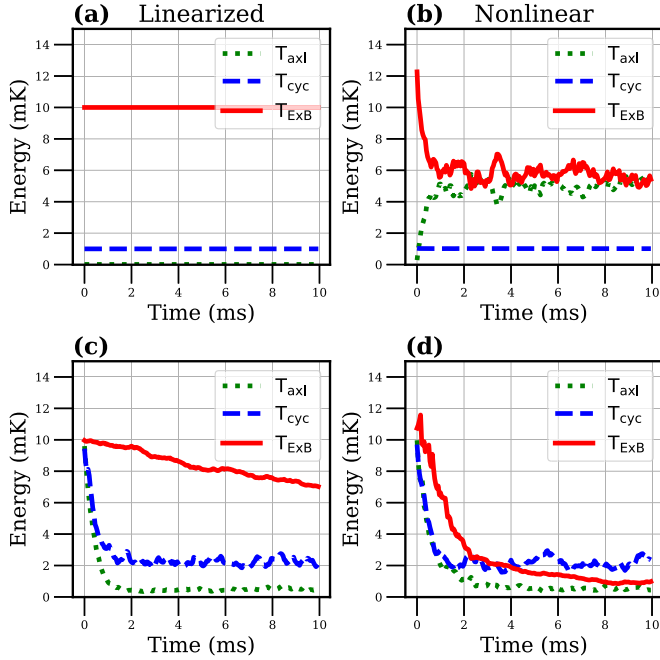
FIG. 3. Comparison of linearized and full simulations. Linearized and full nonlinear simulations for a $N = 54$ ion crystal with $\frac{\delta}{\beta} = 0.25$ and $\omega_r/2\pi = 204$ kHz are evolved with and without laser cooling. (a) Linearized, without laser cooling, no change in mode branch temperatures observed. (b) Nonlinear, without laser cooling, rapid equilibration of $\mathbf{E} \times \mathbf{B}$ and drumhead modes observed. (c) Linearized, with laser cooling, very modest reduction in $\mathbf{E} \times \mathbf{B}$ mode temperature occurs. (d) Nonlinear, with laser cooling, $\mathbf{E} \times \mathbf{B}$ mode temperature reduced to roughly 1 mK.

simulation where the Coulomb interaction, given by the last term in Eq. (1), was expanded to second order in the displacements of the ions from their equilibrium positions. The expansion results in a Coulomb force that is linear in the displacements of the ions. This linearization removes the mode coupling due to higher-order terms, and allows for the direct laser cooling to be isolated in simulations. The details of the linearization procedure and the associated simulations are provided in the SM.

Figure 3 compares the results of the linearized and the full-dynamics (nonlinear) simulations for an $N = 54$ ion crystal at a rotating wall frequency of $\omega_r/(2\pi) = 204$ kHz in the presence and absence of laser cooling. Furthermore, the mode branch temperatures in Fig. 3 are calculated directly from the amplitudes of the modes during evolution. These mode energy averages, neglecting nonlinear corrections from the Coulomb potential, provide an approximation of the system's energy at low temperatures. The mode initialization procedure and calculation of the mode branch temperatures are discussed in Ref. [37] and summarized in the SM.

In Figs. 3(a) and 3(b), we investigate the free evolution of the crystal in the absence of the cooling lasers. The ion crystal was initialized with $\mathbf{E} \times \mathbf{B}$ modes at 10 mK, cyclotron modes at 1 mK, and drumhead modes at 0 mK. In Fig. 3(a), mode branch temperatures are unchanged over 10 ms of free evolution, since the linearization of the dynamics removes the mode coupling and energy cannot be exchanged between

the different branches. In Fig. 3(b), the equilibration of the $\mathbf{E} \times \mathbf{B}$ and drumhead modes occurs rapidly, in roughly 1 ms, demonstrating the strong mode coupling arising from the full nonlinear evolution. We note that the $\mathbf{E} \times \mathbf{B}$ temperatures plotted in Figs. 3(b) and 3(d) exceed 10 mK due to nonlinear corrections neglected in the mode energy calculation, particularly significant for low-frequency $\mathbf{E} \times \mathbf{B}$ modes at energies around 10 mK.

In Figs. 3(c) and 3(d), the linearized and nonlinear simulations were integrated with laser cooling. The nonlinear simulation shown in Fig. 3(d) is the same as the one shown in Fig. 2(d), although in Fig. 3(d) mode branch temperatures are plotted instead of KE$_\parallel$, KE$_\perp$, and PE. In the linearized case, although there is a reduction in the $\mathbf{E} \times \mathbf{B}$ mode temperature during the 10 ms of laser cooling, this temperature is still many times larger than the cyclotron and drumhead mode temperatures. In contrast, in the nonlinear simulation, the $\mathbf{E} \times \mathbf{B}$ mode temperature is rapidly reduced to roughly 1 mK after 10 ms of laser cooling. The difference between the linear and nonlinear simulations further illustrates that coupling between the $\mathbf{E} \times \mathbf{B}$ and drumhead modes due to the nonlinear Coulomb interaction is responsible for the accelerated cooling of the $\mathbf{E} \times \mathbf{B}$ modes.

So far, we compared the cooling dynamics at two representative values of ω_r and demonstrated the role of the mode coupling when ω_r is close to ω_{crit}. To further investigate the effect of mode coupling on the cooling of the $\mathbf{E} \times \mathbf{B}$ modes, we studied the cooling dynamics and mode coupling as ω_r was scanned. In Fig. 4, an $N = 100$ ion crystal was initialized and evolved for a range of rotating wall frequencies between $\omega_r/(2\pi) = 180$ kHz and $\omega_r/(2\pi) = 194$ kHz. The larger number of ions lowers the critical rotating wall frequency to roughly $\omega_{\mathrm{crit}}/(2\pi) = 194.75$ kHz.

In Fig. 4(a), the drumhead and $\mathbf{E} \times \mathbf{B}$ mode frequencies are plotted as ω_r is scanned, with the color gradient specifying the ω_r value. Notably, the lower-frequency drumhead modes are rapidly brought into resonance with the higher end of the $\mathbf{E} \times \mathbf{B}$ branch as ω_r approaches within a few kHz of ω_{crit}. The $\mathbf{E} \times \mathbf{B}$ mode frequencies, however, only change slightly as ω_r is increased.

In Fig. 4(b), we study the energy exchange between the $\mathbf{E} \times \mathbf{B}$ and drumhead mode branches when the crystal is freely evolved in the absence of cooling lasers for 10 ms. Here, the $\mathbf{E} \times \mathbf{B}$ mode branch is initialized with a temperature of 10 mK while the other modes are initialized to 0 mK. We plot the average KE$_\parallel$ during the last 1 ms of the simulation as a function of ω_r. The linearized simulation shows no change in KE$_\parallel$, whereas the nonlinear simulation shows an increase in the average KE$_\parallel$ as ω_r is increased. Near ω_{crit}, KE$_\parallel$ increases to roughly 2.5 mK, which is consistent with the drumhead branch temperature being roughly 5 mK. This suggests that the $\mathbf{E} \times \mathbf{B}$ and drumhead branches equilibrate within 10 ms for ω_r close to ω_{crit}. However, for lower ω_r, KE$_\parallel$ in both the linear and nonlinear simulations is unchanged, indicating that the coupling between branches only becomes significant near ω_{crit}.

In Fig. 4(c), the simulation was integrated with laser cooling for 10 ms. The average total potential energy during the last 1 ms of the simulation is plotted as a function of ω_r. The linearized simulation shows a modest reduction in PE
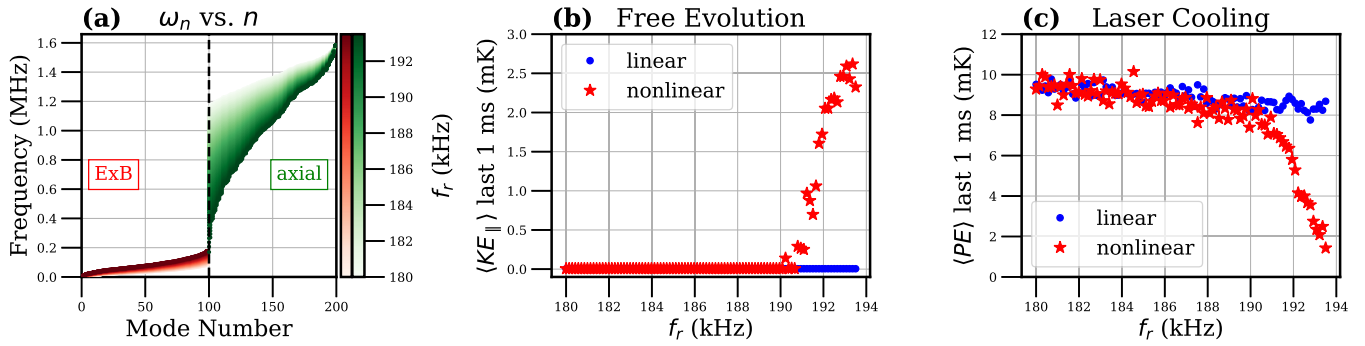
FIG. 4. Rotating wall frequency scan. (a) The $\mathbf{E} \times \mathbf{B}$ and drumhead mode frequencies vs mode number colored by the rotating wall frequency for a $N = 100$ ion crystal. (b) The axial kinetic energy averaged over the last millisecond of evolution vs rotating wall frequency for a $N = 100$ ion crystal evolved for 10 ms without laser cooling (free evolution). The simulations are initialized with $\mathbf{E} \times \mathbf{B}$ mode branch temperatures of 10 mK, and zero drumhead and cyclotron mode branch temperatures. (c) The potential energy averaged over the last millisecond of evolution vs rotating wall frequency for a $N = 100$ ion crystal evolved for 10 ms with laser cooling. The simulations are initialized with all mode amplitudes corresponding to a temperature of 10 mK.

as the ω_r is increased, which may be due to the increased fraction of $KE_\perp$ contributing to the $\mathbf{E} \times \mathbf{B}$ mode energies. However, in the nonlinear simulation, PE is rapidly reduced as ω_r approaches ω_{crit}. Near ω_{crit}, the average PE over the last 1 ms is roughly 1 mK.

Conclusion and outlook. We have demonstrated a technique to efficiently cool the low-frequency planar motion of large two-dimensional (2D) ion crystals in Penning traps, which has hitherto been challenging. Our technique has no experimental overhead and can be used to rapidly initialize (<10 ms) crystals with all motional degrees of freedom cooled down to millikelvin temperatures. This achievement sets the stage for sub-Doppler limit laser cooling studies encompassing all $3N$ motional modes. Furthermore, we showed how the improved planar cooling greatly reduced the spectral broadening of the drumhead modes. The improved resolution of the drumhead modes expands the scope of quantum information protocols that can be performed with large 2D crystals stored in Penning traps. As a result, it is immediately relevant for several experiments aiming to use Penning traps for quantum information processing [2,4,6].

We note that overlapping the bandwidth of the drumhead modes with the $\mathbf{E} \times \mathbf{B}$ modes introduces low-frequency drumhead modes. For a given temperature of the drumhead motion this results in correspondingly larger Lamb-Dicke confinement parameters, which can impact the fidelity of quantum operations [41,42]. Ground-state cooling of the drumhead modes can help [43–45], but experimental constraints may

dictate a lower bound on the drumhead mode frequencies that is significantly higher than any of the $\mathbf{E} \times \mathbf{B}$ modes. In this case it may be possible to use appropriate time-dependent electric field configurations to couple the $\mathbf{E} \times \mathbf{B}$ modes to either the drumhead modes or the cyclotron modes, which are efficiently laser cooled. Techniques like this have been investigated with single and small numbers of trapped ions [25,38]. A notable example is the so-called axialization technique, which reduces the size of the magnetron motion of a small number of ions in a Penning trap by coupling the magnetron motion with the cyclotron motion [7,39,46]. Alternately, there is the possibility of adiabatically decreasing ω_r or similarly increasing ω_z after cooling the $\mathbf{E} \times \mathbf{B}$ modes, which not only eliminates the nonlinear coupling introduced, but would also increase the frequency of the lowest-frequency drumhead modes. These possibilities motivate interesting directions for future numerical simulations.

[1] C. Monroe, W. C. Campbell, L.-M. Duan, Z.-X. Gong, A. V. Gorshkov, P. W. Hess, R. Islam, K. Kim, N. M. Linke, G. Pagano, P. Richerme, C. Senko, and N. Y. Yao, Rev. Mod. Phys. **93**, 025001 (2021).

[2] B. J. McMahon, C. Volin, W. G. Rellergert, and B. C. Sawyer, Phys. Rev. A **101**, 013408 (2020).

[3] B. J. McMahon and B. C. Sawyer, Phys. Rev. Appl. **17**, 014005 (2022).

[4] H. Ball, C. D. Marciniak, R. N. Wolf, A. T.-H. Hung, K. Pyka, and M. J. Biercuk, Rev. Sci. Instrum. **90**, 053103 (2019).

[5] R. N. Wolf, J. H. Pham, J. Y. Z. Jee, A. Rischka, and M. J. Biercuk, arXiv:2303.10801.

[6] J. G. Bohnet, B. C. Sawyer, J. W. Britton, M. L. Wall, A. M. Rey, M. Foss-Feig, and J. J. Bollinger, Science **352**, 1297 (2016).

[7] P. Hrmo, M. K. Joshi, V. Jarlaud, O. Corfield, and R. C. Thompson, Phys. Rev. A **100**, 043414 (2019).

[8] S. Jain, J. Alonso, M. Grau, and J. P. Home, Phys. Rev. X **10**, 031027 (2020).

[9] J. F. Goodwin, B. J. Brown, G. Stutter, H. Dale, R. C. Thompson, and T. Rudolph, Phys. Rev. A **92**, 032314 (2015).

[10] J. W. Britton, B. C. Sawyer, A. C. Keith, C.-C. J. Wang, J. K. Freericks, H. Uys, M. J. Biercuk, and J. J. Bollinger, Nature (London) **484**, 489 (2012).

[11] A. Safavi-Naini, R. J. Lewis-Swan, J. G. Bohnet, M. Gärttner, K. A. Gilmore, J. E. Jordan, J. Cohn, J. K. Freericks, A. M. Rey, and J. J. Bollinger, Phys. Rev. Lett. **121**, 040503 (2018).

[12] J. Cohn, A. Safavi-Naini, R. J. Lewis-Swan, J. G. Bohnet, M. Gärttner, K. A. Gilmore, J. E. Jordan, A. M. Rey, J. J. Bollinger, and J. K. Freericks, New J. Phys. **20**, 055013 (2018).

[13] A. Shankar, E. A. Yuzbashyan, V. Gurarie, P. Zoller, J. J. Bollinger, and A. M. Rey, PRX Quantum **3**, 040324 (2022).

[14] M. Qiao, Z. Cai, Y. Wang, B. Du, N. Jin, W. Chen, P. Wang, C. Luan, E. Gao, X. Sun, H. Tian, J. Zhang, and K. Kim, arXiv:2204.07283.

[15] M. Gärttner, J. G. Bohnet, A. Safavi-Naini, M. L. Wall, J. J. Bollinger, and A. M. Rey, Nat. Phys. **13**, 781 (2017).

[16] B. Swingle, G. Bentsen, M. Schleier-Smith, and P. Hayden, Phys. Rev. A **94**, 040302 (2016).

[17] K. A. Gilmore, J. G. Bohnet, B. C. Sawyer, J. W. Britton, and J. J. Bollinger, Phys. Rev. Lett. **118**, 263602 (2017).

[18] M. Affolter, K. A. Gilmore, J. E. Jordan, and J. J. Bollinger, Phys. Rev. A **102**, 052609 (2020).

[19] L. Pezzè, A. Smerzi, M. K. Oberthaler, R. Schmied, and P. Treutlein, Rev. Mod. Phys. **90**, 035005 (2018).

[20] K. A. Gilmore, M. Affolter, R. J. Lewis-Swan, D. Barberena, E. Jordan, A. M. Rey, and J. J. Bollinger, Science **373**, 673 (2021).

[21] F. Toscano, D. A. R. Dalvit, L. Davidovich, and W. H. Zurek, Phys. Rev. A **73**, 023803 (2006).

[22] A. Shankar, C. Tang, M. Affolter, K. Gilmore, D. H. E. Dubin, S. Parker, M. J. Holland, and J. J. Bollinger, Phys. Rev. A **102**, 053106 (2020).

[23] C. Tang, D. Meiser, J. J. Bollinger, and S. E. Parker, Phys. Plasmas **26**, 073504 (2019).

[24] See Supplemental Material at http://link.aps.org/supplemental/10.1103/PhysRevA.109.L021102 for information on the simulations, ion trap parameters, linearization technique, eigenmode analysis and initialization, and long-time laser cooling simulation results.

[25] L. S. Brown and G. Gabrielse, Rev. Mod. Phys. **58**, 233 (1986).

[26] M. Kretzschmar, Eur. J. Phys. **12**, 240 (1991).

[27] W. M. Itano and D. J. Wineland, Phys. Rev. A **25**, 35 (1982).

[28] R. C. Thompson and J. Papadimitriou, J. Phys. B: At. Mol. Opt. Phys. **33**, 3393 (2000).

[29] M. Asprusten, S. Worthington, and R. C. Thompson, Appl. Phys. B **114**, 157 (2014).

[30] M. van Eijkelenborg, K. Dholakia, M. Storkey, D. Segal, and R. Thompson, Opt. Commun. **159**, 169 (1999).

[31] E. S. Phillips, R. J. Hendricks, A. M. Abdulla, H. Ohadi, D. R. Crick, K. Koo, D. M. Segal, and R. C. Thompson, Phys. Rev. A **78**, 032307 (2008).

[32] W. M. Itano, L. R. Brewer, D. J. Larson, and D. J. Wineland, Phys. Rev. A **38**, 5698 (1988).

[33] J. J. Bollinger, J. N. Tan, W. M. Itano, D. J. Wineland, and D. H. E. Dubin, Phys. Scr. **T59**, 352 (1995).

[34] S. B. Torrisi, J. W. Britton, J. G. Bohnet, and J. J. Bollinger, Phys. Rev. A **93**, 043421 (2016).

[35] X.-P. Huang, J. J. Bollinger, T. B. Mitchell, W. M. Itano, and D. H. E. Dubin, Phys. Plasmas **5**, 1656 (1998).

[36] D. H. E. Dubin, Phys. Plasmas **27**, 102107 (2020).

[37] C. Tang, A. Shankar, D. Meiser, D. H. E. Dubin, J. J. Bollinger, and S. E. Parker, Phys. Rev. A **104**, 023325 (2021).

[38] P.-Y. Hou, J. J. Wu, S. D. Erickson, G. Zarantonello, A. D. Brandt, D. C. Cole, A. C. Wilson, D. H. Slichter, and D. Leibfried, arXiv:2308.05158.

[39] R. J. Hendricks, E. S. Phillips, D. M. Segal, and R. C. Thompson, J. Phys. B: At. Mol. Opt. Phys. **41**, 035301 (2008).

[40] D. H. E. Dubin, Phys. Rev. Lett. **71**, 2753 (1993).

[41] D. Wineland, C. Monroe, W. Itano, D. Leibfried, B. King, and D. Meekhof, J. Res. Natl. Inst. Stand. Technol. **103**, 259 (1998).

[42] A. Sørensen and K. Mølmer, Phys. Rev. A **62**, 022311 (2000).

[43] E. Jordan, K. A. Gilmore, A. Shankar, A. Safavi-Naini, J. G. Bohnet, M. J. Holland, and J. J. Bollinger, Phys. Rev. Lett. **122**, 053603 (2019).

[44] A. Shankar, E. Jordan, K. A. Gilmore, A. Safavi-Naini, J. J. Bollinger, and M. J. Holland, Phys. Rev. A **99**, 023409 (2019).

[45] D. Kiesenhofer, H. Hainzer, A. Zhdanov, P. C. Holz, M. Bock, T. Ollikainen, and C. F. Roos, PRX Quantum **4**, 020317 (2023).

[46] H. F. Powell, D. M. Segal, and R. C. Thompson, Phys. Rev. Lett. **89**, 093003 (2002).